Catalysis Science & Technology

ROYAL SOCIETY OF CHEMISTRY

PAPER

View Article Online
View Journal | View Issue

Cite this: *Catal. Sci. Technol.*, 2025, **15**, 1525

Copper-boosted thiol-functionalized carbon nanospheres from biomass: a novel non-noble metal based recoverable catalyst for efficient nitro-to-amine reduction†

Apoorva Shetty,[ab] Braja Gopal Bag,[c] Uraiwan Sirimahachai[d] and Gurumurthy Hegde *[ab]

In this work, the synthesis and catalytic activity of thiol-functionalized copper-deposited porous carbon derived from dry oil palm leaves (Cu/TF-CNS) was investigated for the reduction of aromatic nitro compounds. The procedure to synthesize porous carbon nanospheres involves the pyrolysis of oil palm leaves in a nitrogen atmosphere at 1000 °C. The resulting porous carbon material was further functionalized with thiol groups to facilitate the uniform deposition of copper nanoparticles and serve as an efficient support. Excellent catalytic performance was shown by the Cu/TF-CNS catalyst in reducing aromatic nitro compounds to their corresponding aromatic amines with a low copper loading of only 4 mol% which is an inexpensive non-noble metal in the presence of $NaBH_4$ as a reducing agent and EtOH/H_2O as green solvents. The products were identified using ^1H NMR spectroscopy. The catalyst was isolated from the reaction mixture and reused upto 10 cycles without any significant loss in the activity. The ICPAES analysis confirmed the successful incorporation of approximately 8.9% Cu during the deposition process and the reusability of the catalyst underscores its efficacy as a sustainable and effective heterogeneous catalyst for nitroarene reduction.

Received 12th November 2024,
Accepted 20th January 2025

DOI: 10.1039/d4cy01368a

rsc.li/catalysis

Introduction

Driven by environmental concerns and green chemistry objectives, chemists strive to devise novel pathways for the elimination or reduction of pollutants, utilizing waste materials for synthesizing valuable chemicals. Nitro compounds, prevalent in industrial and agricultural wastewater, are deemed toxic environmental pollutants. A viable solution involves catalytic reduction of nitro compounds to yield amines, which are valuable entities in synthetic organic chemistry.[1,2]

The catalytic reduction of aromatic nitro compounds remains attractive due to its widespread use in synthesizing intermediates and final products across various sectors such as dyes, agricultural chemicals, pharmaceuticals, and materials, both in laboratory and industrial settings. Despite numerous reported synthetic routes for aniline preparation from corresponding aromatic nitro compounds, there persists a need for the development of cost-effective catalysts with high activity.

The conventional method of producing amines involves reacting free hydrogen gas with the nitro groups while using either heterogeneous or homogeneous catalysts. However, because of the severe reaction conditions, including high temperatures and pressures this conventional procedure poses a higher risk.[3–5] To address safety concerns, alternative hydrogen sources such as hydrazines, formic acid, alcohol derivatives, including glycerol, isopropanol, and ethanol have garnered interest. Although these alternatives are safer, environmentally friendly, and require less stoichiometric amounts, their hydrogenation process tends to be slow and occasionally demands elevated temperatures.[6] Thus, sodium borohydride ($NaBH_4$) is regarded as the best option for reducing R–NO_2 to R–NH_2, acting as a possible source of hydrogen.[7] Sodium borohydride hydrolysis is a useful source of hydrogen due to its high volumetric density (10.8 wt% hydrogen content), excellent stability, and safety.[3] The conventional use of sodium borohydride typically involves noble metal activators such as silver, platinum, or palladium.[8,9]

[a] *Department of Chemistry, Christ University, Hosur Road, Bangalore 560029, India*
[b] *Centre for Advanced Research and Development (CARD), Christ University, Hosur Road, Bangalore 560029, India. E-mail: murthyhegde@gmail.com*
[c] *Department of Chemistry & Chemical Technology, Vidyasagar University, Midnapore 721102, West Bengal, India*
[d] *Department of Chemistry and Centre of Excellence for Innovation in Chemistry, Faculty of Science, Prince of Songkla University, Hat Yai, Songkla 90112, Thailand*
† Electronic supplementary information (ESI) available. See DOI: https://doi.org/10.1039/d4cy01368a

The strategy of employing metals as catalysts in organic reactions has a century-old tradition. Metallic nanoparticles, distinguished by unique physico-chemical properties attributed to a higher surface atom count, have garnered significant attention.[10,11] Recently, noble metal-free alternatives have emerged, aiming to advance more sustainable chemical processes.[8,12]

Copper nanoparticles (CuNPs) are particularly appealing due to their abundant natural availability and cost-effectiveness. The simple and productive methods of preparing these Cu-based nanomaterials add to their attractiveness.[13] Copper, as a versatile transition metal, can exist in various oxidation states (Cu^0, Cu^I, Cu^{II}, and Cu^{III}), enabling diverse reactions through both one- and two-electron pathways. The unique characteristics of Cu-based nanocatalysts find applications in nanotechnology, including catalytic organic transformations, electrocatalysis, and photocatalysis.[13,14]

In reduction reactions specifically, the active site of Cu exhibits strong affinity for hydrogen atoms and other molecules, which prolongs the lifespan of reactive species and increases the potential for reactions.[15] However, to address potential issues such as aggregation in aqueous media, a promising approach involves the development of solid supports for the immobilization and stabilization of nanoparticles.[10] Over time, the research emphasis has also been towards the development of supports, which is often more cost-effective and environmentally sustainable compared to focusing on active species. This aspect renders the field highly appealing with substantial potential. A fundamental approach to altering support properties involves manipulating their size and shape, achieved through downsizing into nanoparticles. This modification significantly impacts the resulting catalytic properties, enabling precise adjustments for the preferential exposure of specific active sites. Such modifications aim to maximize the availability of active sites for reagents, enhance overall activity, and guide the reaction towards the formation of a desired product, thereby achieving greater selectivity.[16,17]

In heterogeneous catalysis, porous solids serve as supports that facilitate the even dispersion of active metal or metal oxide catalysts while also helping to lower the overall cost of the catalyst.[18] A wide range of support materials are available, including amorphous oxides, nanoporous crystalline oxides (zeolites), mesoporous oxides, and others.[19] However, carbon based materials have found numerous applications in heterogeneous catalysis because of their abundance and low cost.[20] Among these, nanocarbons stand out due to their numerous advantages, such as large surface area, high adsorption capacity, remarkable stability in aggressive media (acidic or basic), excellent thermal and mechanical stability, outstanding electronic properties, tunable porosity, and the ability to effectively anchor and disperse active metal nanoparticles.[19,21] These properties enable nanocarbons to perform versatile functions. Hence significant research efforts continue to explore and unravel the fascinating chemistry of nanocarbon materials.[22]

The utilization of low-cost waste materials, such as lignocellulose,[23] bagasse,[24,25] and chitosan,[26,27] for the synthesis of such carbonaceous supports/materials is imperative. These materials, characterized by both economic viability and environmental benignity, play a crucial role as raw materials in facilitating advanced catalytic transformations.

Using carbon as a support for heterogeneous catalysts presents significant challenges due to its complex surface characteristics and the potential for surface modification through various treatments.[28] Introducing heteroatoms can create defects that modify the surface structure, providing anchoring points for metal nanoparticles or active sites.[29,30] Chemical functionalization of nanocarbons is thus a valuable approach for introducing uniformly distributed anchoring points.[31] Additionally, modified carbons often exhibit reduced aggregation compared to their pristine forms, resulting in improved dispersibility and enhanced catalytic performance.[32] Sulfur-containing functional groups, particularly thiol (–SH), have attracted special attention due to their strong affinity for transition metals, making them effective for anchoring metal nanoparticles.[33,34]

In this study, we investigated the potential of using a low loading (4 mol%) of affordable Cu to develop a biomass derived thiol functionalized catalyst Cu/TF-CNS with good efficiency, yield, stability and recyclability for nitro amine reduction reactions. The porous carbons were synthesized from dry oil palm leaves at 1000 °C through a pyrolysis technique providing an efficient carbon support. Thiol functional groups were introduced onto the carbon *via* a chemical functionalization technique, and copper nanoparticles were then immobilized onto the porous nanocarbons, resulting in the formation of the Cu/TF-CNS catalyst. The effectiveness of Cu/TF-CNS was tested under different reaction conditions using the model reduction of 4-nitroaniline. Additionally, its versatility and recyclability were examined to determine its practical potential as an efficient heterogeneous catalyst. This study aims to deepen our understanding of the potential of using low-cost metals like copper effectively, as well as the impact of functionalization on the stability, recyclability and catalytic performance, thereby providing promising implications for developing cost-effective and sustainable materials.

Experimental

Materials and methods

The aromatic nitro compounds utilized in this study were sourced from Avra Synthesis Pvt Ltd and used without additional purification. Ethanol was procured from Finar Chemicals. All other chemicals, including thionyl chloride, 2-mercaptoethanol, $CuCl_2{\cdot}2H_2O$, and sodium borohydride were sourced from Chempure.

Preparation of materials

Synthesis of the carbon nanospheres (OPL-CNS). The dry oil palm leaves were obtained from various oil palm cultivation farms across India. The leaves were washed to remove dust particles and then dried in a hot air oven at 100 °C for about 24 h. This biowaste precursor was then powdered and sieved to 60 μm. The powdered material was placed in a silica crucible and carbonized under a N_2 atmosphere at 1000 °C in a quartz tube furnace, with a constant nitrogen flow maintained throughout the synthesis. The pyrolyzed carbon was then washed thoroughly with 0.1 N HCl, followed by water, and then dried to obtain OPL-CNS, which was used for further studies.[35,36]

Preparation of thiol functionalized CNSs (TF-CNS). The synthesized OPL-CNS (1 g) was dispersed in a mixture of 50 mL of HNO_3 and H_2SO_4 taken in a 1 : 3 ratio and sonicated at 40 °C for about 3 h. The reaction mixture was then diluted with 100 mL of distilled water, washed thoroughly, filtered, and dried at 45 °C in a hot air oven for 8 h to obtain acid functionalized carbon nanospheres (AF-CNS) (Scheme 1, step 1). The acid-functionalized carbon nanospheres (AF-CNS) 800 mg, were taken in 6 mL of DMF. To this, 150 mL of $SOCl_2$ was added and refluxed at 60 °C for 24 h. The reaction mixture was then concentrated in a rotary evaporator to remove excess $SOCl_2$, washed with 40 mL THF, dried and taken to the next step immediately (Scheme 1, step 2).

About 100 mL of ACN was added to the activated acid functionalized carbon nanospheres (AF-CNS) taken in a 500 mL round bottom flask. To this, about 3 mL of DIPEA and 3 mL of 2-mercaptoethanol were added and stirred at RT for 3 h. The reaction mixture was then heated at 65 °C for 12 h. Upon the completion of the reaction, it was cooled to RT, and the solid was allowed to settle and washed with about 50 mL of water followed by 50 mL of ethanol, dried in a hot air oven at 50 °C for about 8 h to obtain thiol functionalized carbon nanospheres (TF-CNS). (Scheme 1, step 3).

Preparation of Cu-deposited thiol functionalized CNSs (Cu/TF-CNS). The synthesized TF-CNS (1 g) was taken in a 250 mL beaker, dispersed in 50 mL of DI water, sonicated for 30 min to obtain a uniform dispersion. To this, a solution of 10 wt% of $CuCl_2{\cdot}2H_2O$ in 50 mL of DI water was added and sonicated for 30 min. Further, 50 mL of 1% of sodium borohydride was added dropwise to reduce Cu(II) to Cu(0). The suspension was stirred at RT for about 16 h. The suspension was allowed to settle, filtered, washed thoroughly with 100 mL of distilled water followed by 100 mL of ethanol, and dried in an oven at 50 °C for 6 h to obtain Cu-deposited thiol functionalized CNSs (Cu/TF-CNS). (Scheme 1, step 4).

Material characterization

To determine the morphology of the samples and confirm the presence and relative abundance of elements in OPL-CNS and Cu/TF-CNS, field emission scanning electron microscopy (SEM) was performed with an Apreo (Thermo Fisher Scientific) operated at an accelerating voltage of 20.0 kV and transmission electron microscopy (TEM) was performed using a JEOL JEM-2010. The elemental composition and the binding energy of the sample constituents were determined using X-ray photoelectron spectroscopy (XPS, Thermo/ESCALAB 250XI). X-ray diffraction (XRD) patterns were obtained using a Rigaku Miniflex 600 employing Cu-Kα radiation. The Cu loading in Cu/TF-CNS and recycled Cu/TF-CNS was measured by inductively coupled plasma analysis (ICPAES, ARCOS, SPECTRO Analytical Instruments GmbH). For the Cu/TF-CNS catalyst optimization study, the crude reaction mixtures were analyzed by gas chromatography (GCMS-QP2010 SE, SHIMADZU). The isolated aromatic amine derivatives were characterized by ^1H and ^{13}C NMR

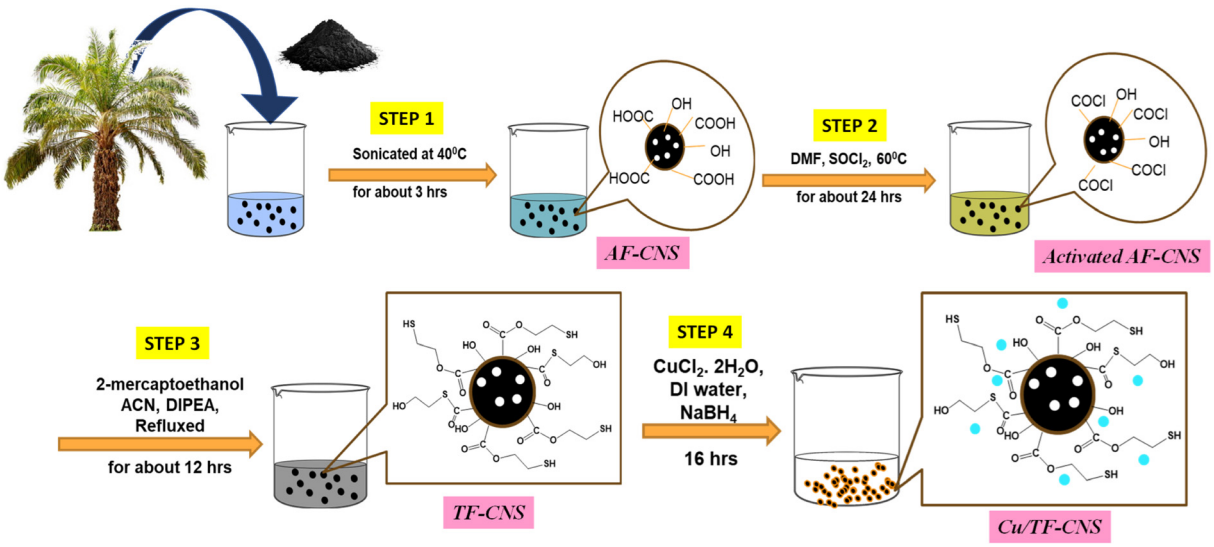

Scheme 1 Schematic representation for the synthesis of OPL-CNS followed by the synthesis of Cu/TF-CNS.

spectroscopy (Bruker Ascend 400 MHz) using dimethyl sulfoxide-d_6 (DMSO-D_6) as the solvent.‡

General procedure for the nitroarene reduction reaction using the Cu/TF-CNS catalyst

In a 25 ml vial containing 3 mL of an appropriate solvent placed on a magnetic stirrer, a nitroaromatic compound (1 mmol) was added. The catalyst Cu/TF-CNS (20 wt%) was then introduced to the reaction mixture, followed by the addition of $NaBH_4$ (5 mmol). The reaction mixture was stirred continuously at 80 °C, with the progress monitored periodically by TLC. Upon completion, the Cu/TF-CNS catalyst was separated from the mixture *via* centrifugation. The reaction mixture was then diluted with water, and the organic layer was extracted with ethyl acetate (3 × 5 ml) and dried over anhydrous Na_2SO_4. The organic solvent was evaporated under vacuum to yield the crude product, which was purified using column chromatography on silica gel (60–120 mesh) using an ethyl acetate : hexane mobile phase. The product formation was confirmed by recording the ^{1}H NMR spectra.

Procedure for the reuse of the catalyst

After the reaction was complete, (2 × 5 mL) of ethyl acetate was added to the reaction mixture and stirred for 5 minutes. The catalyst was then separated from the mixture using centrifugation. The isolated solid was thoroughly washed with water (5 mL), followed by ethanol (5 mL) and then dried under reduced pressure. This recovered catalyst was subsequently used for another reaction run, demonstrating its reusability and suitability for multiple reaction runs.

Results and discussion

Characterization of the Cu/TF-CNS catalyst

Scheme 1 shows the steps related to the synthesis of the Cu/TF-CNS nanocatalyst. The OPL-CNS was synthesized at 1000 °C from dry oil palm leaves, resulting in the formation of mesoporous spherical carbons, which acted as efficient eco-friendly supports for the synthesis of the catalyst. Carboxyl groups were grafted onto the OPL-CNSs after oxidizing them using a mixture of HNO_3/H_2SO_4, taken in a ratio of 1 : 3 to obtain AF-CNS and then, addition of thionyl chloride stimulated it to yield activated AF-CNS for the reaction with 2-mercaptoethanol, introducing sulphur functional groups onto the carbon support (TF-CNS). Finally, copper nanoparticles were deposited on the surface of the thiolated CNS affording the Cu/TF-CNS. Inductively coupled plasma (ICP-AES) analysis determined that the synthesized material contained 8.96% copper, as shown in Table S3 (ESI†).

The Fig. 1a–c illustrate the X-ray diffraction (XRD) patterns, FESEM image with the EDS plot and TEM image of the synthesized OPL-CNS. The XRD pattern of OPL-CNS exhibited two broad peaks around 24° and 44°, corresponding to the (002) and (100) lattice planes of graphitic carbon, (JCDPS card no. 75–1621) respectively.[37] The broad nature of these peaks suggested the formation of an amorphous type of carbon material. The structural characteristics of OPL-CNS were initially analyzed using FESEM, as shown in Fig. 1b, where the CNS displayed a spherical morphology with an average diameter of 62 nm and the EDS analysis of OPL-CNS indicated that carbon accounted for approximately 79% of the composition. The TEM image of OPL-CNS Fig. 1c further confirmed the spherical morphology and revealed an uneven, flake-like structure, potentially contributing to the tendency of the material to form spherical aggregates.[38]

The crystallinity and morphological analysis was performed on the synthesized Cu/TF-CNS catalyst. The XRD pattern of Cu/TF-CNS Fig. 2a confirmed the presence of Cu particles on the carbon substrate. Along the broad peak at approximately 24°, indicative of the (002) facet of amorphous carbon, two sharp peaks were observed at 2θ = 42.4 and 73.7 corresponding to the (111) and (220) planes of fcc metallic Cu (JCPDS no. 04-0836).[39] Additionally, two distinct sharp peaks at 2θ = 36.5 and 61.6 were attributed to the (111) and (220) planes of cubic phases of Cu_2O, (JCPDS no. 78-2076) respectively.[40] The XRD pattern showed that both Cu and Cu_2O coexist in the material and the formation of Cu_2O may be due to the nature of copper readily oxidizing in the presence of air. Fig. 2b presents the FESEM image and EDS profile of Cu/TF-CNS, illustrating the presence of copper particles deposited on the mesoporous carbon, while the carbon has retained its spherical morphology even after the deposition of copper nanoparticles. The EDS profile of the catalytic material Cu/TF-CNS gave the elemental percentages of carbon, oxygen, sulphur and copper to be 63%, 23.8%, 4.5%, and 8.6% respectively. The elemental percentage of copper on TF-CNS, as indicated by the EDS profile, aligns with the amount of copper deposited during the synthesis procedure and is consistent with the ICP-AES analysis data (Table S3, ESI†). The elemental mapping of the Cu/TF-CNS further demonstrated a uniform deposition of copper as well as the uniform functionalization of the carbon surface (Fig. 2d). The TEM image (Fig. 2c) of Cu/TF-CNS further confirms the deposition of copper on TF-CNS; the copper nanoparticles appeared as dark spots on the surface of the carbon.

XPS measurements were conducted to analyze the elemental composition and chemical bonding states of OPL-CNS, and the catalyst Cu/TF-CNS. These measurements provided insights into the oxidation state of the copper species associated with the catalyst under investigation and helped assess the role of copper species that contribute towards catalytic activity. The representative XPS survey spectra for OPL-CNS revealed the presence of C 1s and O 1s peaks, with mass concentrations of approximately 75% for C and 15% for O. Trace amounts of Ca (~3%) and Si (~6%) were also detected in the sample. The well deconvoluted C 1s spectrum (Fig. 3a) consisted of four distinct component peaks corresponding to sp^3 C–C (285 eV), C–O (286 eV), C–O–C (286.8 eV), and C═O (287.9 eV). Similarly, the O 1s spectrum

‡ ^{1}H NMR and ^{13}C NMR data of compounds. ICPAES data for the catalyst (ESI†).

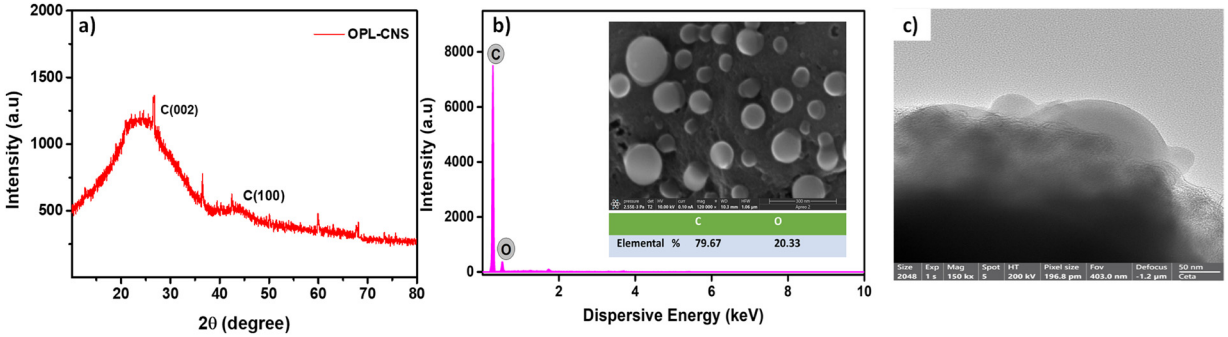

Fig. 1 (a) X-ray diffraction pattern of OPL-CNS, (b) FESEM image along with the EDS plot of OPL-CNS and (c) TEM image of OPL-CNS.

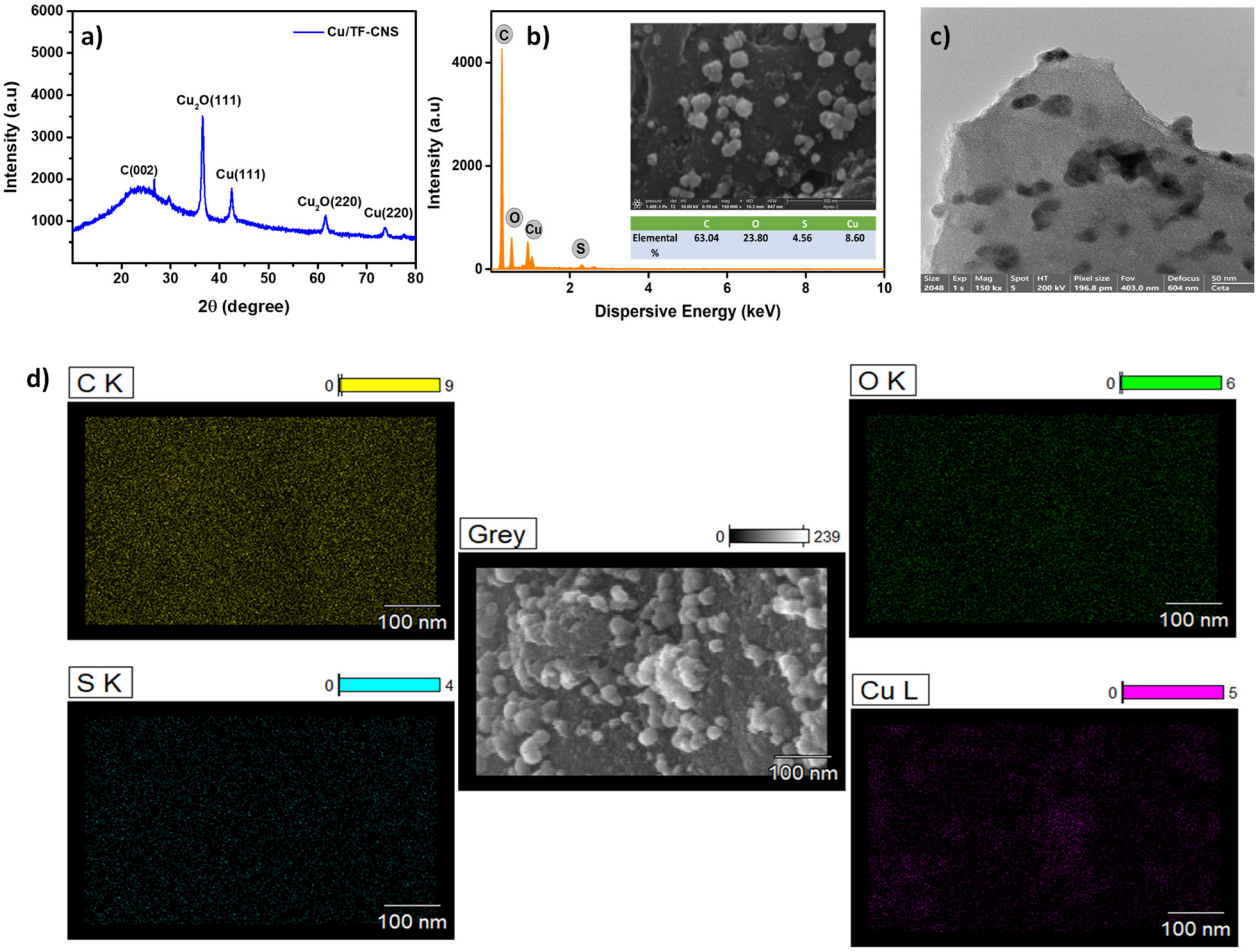

Fig. 2 (a) X-ray diffraction pattern of Cu/TF-CNS, (b) FESEM image along with EDS plot of Cu/TF-CNS, (c) TEM image of Cu/TF-CNS and (d) Cu/TF-CNS; elemental mapping of composition elements C, O, S and Cu.

(Fig. 3b) was deconvoluted into four individual component peaks corresponding to ether C–O–C (531.1 eV), carbonyl oxygen O–C═O (532.19 eV), non-carbonyl oxygen in O═C–O (533.1 eV), and hydroxy O–H (534.4 eV).[38,41] The representative XPS survey spectra for Cu/TF-CNS revealed the presence of C 1s, O 1s, S 2p and Cu 2p peaks. The mass concentrations were found to be 61.8%, 20.3%, 1.8% and 9% for C, O, S, and Cu respectively. The binding energy (BE) of C 1s electrons in the Cu/TF-CNS catalyst was similar to that of OPL-CNS. The well deconvoluted C 1s spectrum (Fig. 3c) contained five distinct component peaks corresponding to sp^3 C–C (285 eV), C–O (285.8 eV), C–O–C (286.8 eV), C═O (287.7 eV) and O–C═O (289.3 eV).[42] However, due to the close binding energy values, the C 1s core spectrum cannot be precisely used to differentiate between the C–O, C–S and the desired C–SH bond. The O 1s spectrum (Fig. 3d) was

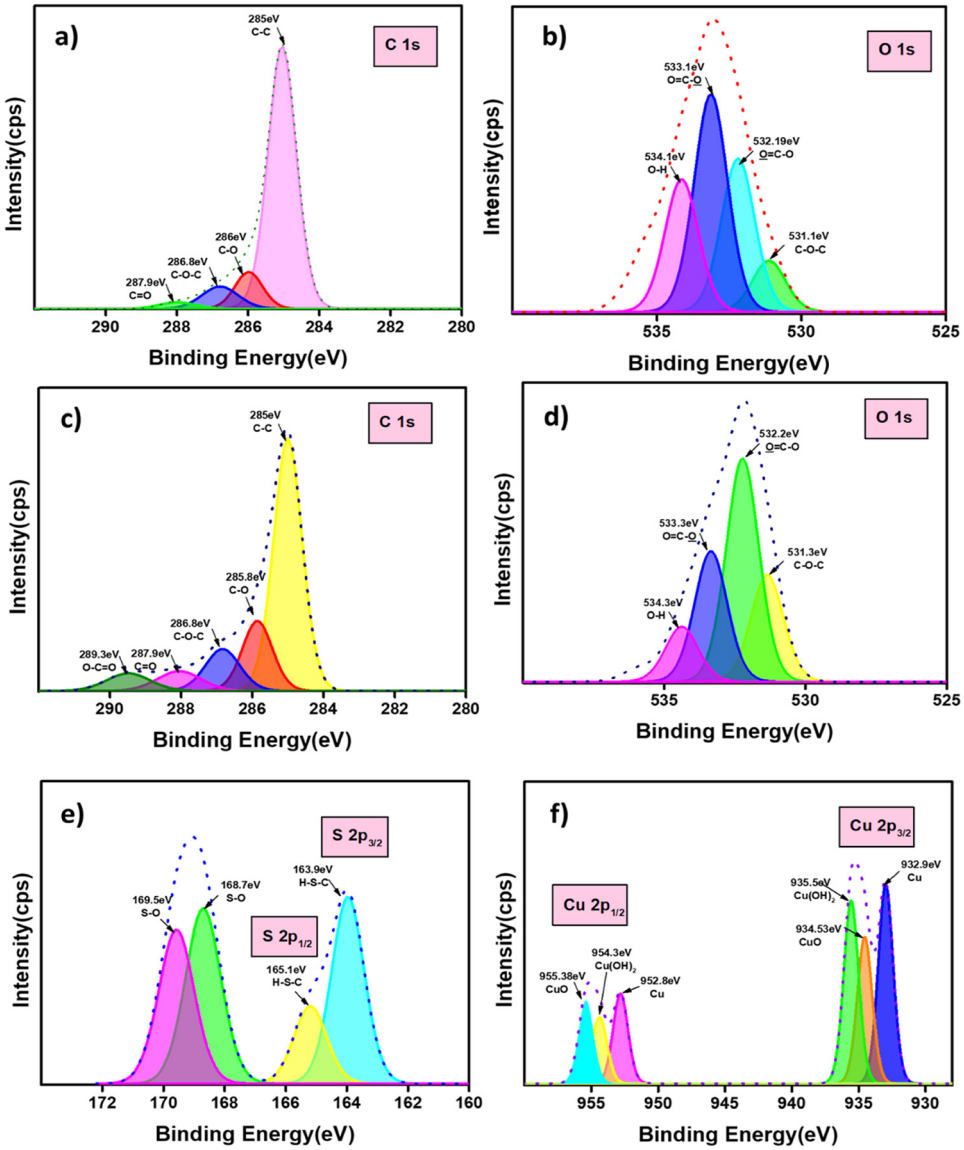

Fig. 3 XPS spectrum: OPL-CNS (a and b) for C 1s and O 1s, respectively, and Cu/TF-CNS (c–f) for C 1s, O 1s, S 2p and Cu 2p, respectively.

deconvoluted into four individual component peaks corresponding to ether C–O–C (531.3 eV), carbonyl oxygen O–C═O (532.2 eV), non-carbonyl oxygen in O═C–O (533.3 eV), and hydroxy O–H (534.4 eV). Notably, there was an increase in percentage area for carbonyl oxygen O–C═O (532.2 eV) as compared to O 1s spectra of OPL-CNS, which may be attributed to the functionalization of the material resulting in an increase in carbonyl oxygen content. The S 2p spectrum (Fig. 3e) is also deconvoluted to reveal two peaks of C–S–H (S 2p) appearing at binding energies of 163.9 eV and 165.1 eV for Cu/TF-CNS,[43] confirming the successful grafting of S–H onto the carbon surface. Additional peaks at 168.7 eV and169.5 eV can be attributed to S–O/O–S–O, likely resulting from the formal oxidation of sulfur during analysis.[44] In the XPS spectra (Fig. 3f), two Cu peaks were observed at binding energies of approximately 932.9 eV and 952.8 eV, corresponding to Cu $2p_{3/2}$ and Cu $2p_{1/2}$, respectively.[45] The presence of CuO (934.5 and 955.3 eV) indicates that copper on the surface can be easily oxidized at room temperature.

Additionally, peaks for $Cu(OH)_2$ (935.5 and 954.4 eV) were also detected.[46,47] The binding energies (BE) of Cu $2p_{3/2}$ and Cu $2p_{1/2}$ electrons in Cu/TF-CNS suggest the presence of both metallic Cu^0 and Cu^{2+} species. The limited energy resolution of X-ray photoelectron spectroscopy (XPS) makes it challenging to differentiate between Cu and Cu_2O since the difference in their $2p_{3/2}$ energies is less than the resolution of the XPS tool.[48] These findings support the efficiency and recyclability of the catalyst in reduction reactions, as the successful functionalization of the support has led to better interaction between the support and the metallic particles, contributing to their effective recyclability and catalytic properties.

Catalytic activity of the Cu/TF-CNS catalyst in the nitro to amine reduction reaction

Optimization studies. To optimize the reaction conditions for the nitro to amine reduction reaction using the Cu/TF-CNS catalyst a series of reactions were performed using ecofriendly solvents such as ethanol and water, different hydrogen sources such formic acid and hydrazine hydrate, different temperatures such as RT, 50 °C and 80 °C and catalyst loadings (5 wt%, 10 wt%, 15 wt%, 20 wt% and 25 wt%) in order to obtain mild and sustainable reaction conditions. All the results obtained from the optimization studies are presented in Table 1.

The optimization studies were performed for the model reaction of the reduction of 4-nitroaniline. The selection of solvents played a crucial role. The aim was to use water as a green solvent since organic solvents tend to cause carcinogenic and genotoxic diseases; however there were some water insoluble starting materials, therefore the EtOH/H_2O system was chosen to facilitate the solubility of such materials. Hence, the choice of solvent was evaluated keeping the hydrogen source ($NaBH_4$), the catalyst loading (20 wt%) and the temperature (80 °C) constant. The experimental results for the reduction of 4-nitroaniline are summarized in Table 1 (entries 1–3), demonstrating promising conversion rates (>99%) for the H_2O system in 20 min, whereas the EtOH system exhibited inadequate conversion, and the EtOH/H_2O solvent system did not yield favorable outcome as compared to the H_2O system in facilitating the reduction reaction; this may be due to the poor solubility of the starting material. Hence due to better conversion rate of the H_2O system, this solvent system was optimized for further investigations.

Further investigations were performed to optimize the catalyst loading. Cu loadings 5 wt%, 10 wt%, 15 wt%, 20 wt% and 25 wt% were considered (Table 1, entries 3–7), keeping the solvent system (H_2O), the hydrogen source ($NaBH_4$) and the temperature (80 °C) constant. After examining the reactions, a 20 wt% loading (4 mol%) of Cu was selected for further studies due to its better product conversion within a shorter reaction time. Additionally, increasing the catalyst loading did not significantly affect the catalytic performance in this study.

In the next phase, the catalytic activity of Cu/TF-CNS was evaluated using $NaBH_4$, formic acid and hydrazine hydrate as different hydrogen sources. Notably, the reaction using $NaBH_4$ as a reducing agent exhibited significantly better conversion rates and yields compared to those using HCOOH and $N_2H_4{\cdot}2H_2O$ which did not yield the desired results (Table 1, entries 3, 8 & 9). This enhanced performance may be attributed to the greater amount of hydride formed and transferred when using $NaBH_4$ in conjunction with the Cu/TF-CNS catalyst under the optimized reaction conditions. Further optimization of the reaction temperature at RT, 50 °C and 80 °C showed that performing the reaction at 80 °C resulted in high conversion rates (Table 1, entries 3, 10 &11). Studies performed to examine the effect of functionalization of the catalyst showed that OPL-CNS (Table 1, entry 12) did not exhibit significant catalytic activity, while Cu/OPL-CNS (Table 1, entry 13), the non-thiol-functionalized catalyst, demonstrated reduced catalytic activity and required longer reaction times as compared to Cu/TF-CNS, the thiol-functionalized catalyst. The results confirmed that chemical functionalization, which introduces heteroatoms, creates uniformly distributed anchoring points for metal nanoparticles due to their stronger affinity for transition metals. This leads to improved dispersibility and enhanced catalytic performance. Subsequently, the role of the Cu/TF-CNS catalyst and the significance of the hydrogen source ($NaBH_4$) were examined. In the absence of a catalyst, the reaction progressed slowly, with a conversion rate of less

Table 1 Optimization of the reaction conditions for nitro-amine catalysis by Cu/TF-CNS

SL. no	Solvent	Catalyst loading (wt%)	Hydrogen source	Temperature	Time	Product conversion
1	EtOH/H_2O	20%	$NaBH_4$	80 °C	50 min	58%[a]
2	EtOH	20%	$NaBH_4$	80 °C	50 min	15%[a]
3	**H_2O**	**20%**	**$NaBH_4$**	**80 °C**	**20 min**	**>99%**[b]
4	H_2O	5%	$NaBH_4$	80 °C	90 min	12%[a]
5	H_2O	10%	$NaBH_4$	80 °C	50 min	>99%[b]
6	H_2O	15%	$NaBH_4$	80 °C	25 min	>99%[b]
7	H_2O	25%	$NaBH_4$	80 °C	20 min	>99%[b]
8	H_2O	20%	HCOOH	80 °C	120 min	2%[a]
9	H_2O	20%	$N_2H_4{\cdot}2H_2O$	80 °C	120 min	No reaction
10	H_2O	20%	$NaBH_4$	RT	150 min	9%[b]
11	H_2O	20%	$NaBH_4$	50 °C	150 min	90%[b]
12	H_2O	20% (Cu/OPL-CNS)	$NaBH_4$	80 °C	60 min	96%[b]
13	H_2O	20% (OPL-CNS)	$NaBH_4$	80 °C	60 min	Trace
14	H_2O	No catalyst	$NaBH_4$	80 °C	120 min	<5%
15	H_2O	20%	No H_2 source	80 °C	120 min	No reaction

Reaction conditions: 4-nitroaniline (1.0 mmol), Cu/TF-CNS, hydrogen source (5 mmol), solvent 3 mL. [a] Product conversion based on GCMS analysis. [b] Isolated yield.

than 5% even after 120 min (Table 1, entry 14), while in the absence of a hydrogen source ($NaBH_4$) the reaction did not occur at all (Table 1, entry 15). These results clearly demonstrate the crucial roles of both the Cu/TF-CNS catalyst and the hydrogen source in facilitating the efficient progress of the reduction reaction.

Reactions. The scope and generality of the catalytic protocol using Cu/TF-CNS were investigated through the reduction of structurally diverse aromatic nitro compounds under optimized conditions with $NaBH_4$ as the reducing agent (Table 2). The detailed results in Table 2 indicate the halogenated nitroarenes were successfully reduced to the corresponding anilines without any dehalogenation, which was a common issue encountered with several hydrogenation reactions (Table 2, entry 6). Molecules featuring both nitro and carbonyl groups showed no selectivity, as both functional groups were reduced with equal reactivity. This was demonstrated by the reduction of nitroacetophenone to the corresponding amino alcohol (Table 2, entry 13). Further investigations revealed that the present method was also effective for reducing dinitroarenes to the corresponding phenylenediamines under the same reaction conditions (Table 2, entry 10). To broaden the scope of the catalyst, various mono substituted aromatic nitro compounds containing –OH in different positions (Table 2, entries 1, 11 & 12), $-NH_2$ in various positions (Table 2, entry 2, 4 & 5), and $-OCH_3$ (Table 2, entry 9) were successfully reduced. Additionally, the disubstituted aromatic nitro compound containing $-OCH_3$ and $-NH_2$ (Table 2, entry 8) as well as the bicyclic nitro compound (Table 2, entry 7) were also converted to their corresponding amines using the Cu/TF-CNS catalyst. Thus, the successful application of the Cu/TF-CNS catalytic system was achieved, yielding favourable results for the desired products, often within a shorter time frame. The spectroscopic data for the corresponding aromatic amines listed in Table 2 are provided in the ESI† (^{1}H NMR, Fig. S1a–m and ^{13}C NMR, Fig. S2a–f).

Recyclability, stability and heterogeneity test of Cu/TF-CNS

The recyclability of the Cu/TF-CNS catalyst was assessed in the reduction reaction of 4-nitroaniline under optimized reaction conditions. After each cycle, the Cu/TF-CNS catalyst was easily recovered from the reaction mixture through centrifugation, followed by washing with water and ethanol, and dried. The recovered Cu/TF-CNS catalyst was used in subsequent cycles. Even after 10 reaction cycles, the product yield and catalytic activity remained high, as shown in Fig. 4. This substantial yield across multiple cycles indicates that the Cu/TF-CNS catalyst is highly efficient and recyclable under the given reaction conditions. The heterogeneity of Cu/TF-CNS was a key focus of investigation, particularly regarding its leaching behavior. ICP-AES analysis of the recycled catalyst revealed that the copper content in the used catalyst remained at 8.9% (Table S3, ESI†) indicating no significant leaching of copper during the reaction, confirming the stability of Cu/TF-CNS under the reaction conditions. Additionally, XRD analysis (Fig. 5a) of the recycled Cu/TF-CNS (R-Cu/TF-CNS) displayed the characteristic peaks for both copper and carbon.

An examination of the morphology of the recycled catalyst using FESEM (Fig. 5b) revealed no significant changes. A hot filtration test was performed to further validate the heterogeneous nature of Cu/TF-CNS. The test demonstrated an approximately 50% conversion rate after 10 minutes, at which point the catalyst was removed from the reaction mixture. The reaction was then allowed to proceed for an additional 150 minutes without the catalyst, and TLC analysis after 2.5 h showed no significant increase in the conversion rate of the desired product. These results affirm the structural stability and heterogeneity of the catalyst.

Table 3 presents a comparative analysis of the catalytic activity of the Cu/TF-CNS catalyst with other previously reported noble and non-noble metal based heterogeneous catalysts for the reduction of 4-nitroaniline to benzene-1,4-diamine. From Table 3, it is evident that Cu/TF-CNS demonstrated favorable results regarding yield and reaction time compared to other catalytic systems. Although some systems achieved high yields, they often required larger quantities of more expensive metals, complex synthesis procedures or relatively longer reaction times. Additionally, the reusable Cu/TF-CNS catalyst offers several advantages including (i) the use of a cost effective, non-noble metal, (ii) high efficiency, excellent recyclability and environmental friendliness due to its operation in green solvents, (iii) enhanced safety, since it does not necessitate any specialized hydrogenation system, and (iv) ease of operation under ambient conditions.

Catalytic mechanism

The porous carbon facilitates rapid electron transfer and molecular diffusion within its structure, similar to other carbon-based materials. This leads to enhanced dipole–dipole interactions around the copper nanoparticles (Cu-NPs), while the thiol functional groups on the carbon help stabilize the copper nanoparticles.[55] Furthermore these functional groups enable efficient adsorption of aromatic nitro compounds by providing various noncovalent interactions, such as π–π stacking and hydrogen bonds. These interactions enhance the accessibility of aromatic nitro compounds to the surface of the Cu/TF-CNS catalyst.[56] Following the comprehensive characterization of Cu/TF-CNS, along with examinations of its stability, recyclability, and heterogeneity as a catalyst in the reduction reaction, we propose a potential mechanism for the complete reduction of aromatic nitro compounds to their corresponding amines on the Cu/TF-CNS surface Scheme 2. Initially, hydrogen is generated from sodium borohydride which is then adsorbed

Table 2 Reduction of various nitroarenes catalyzed by Cu/TF-CNS

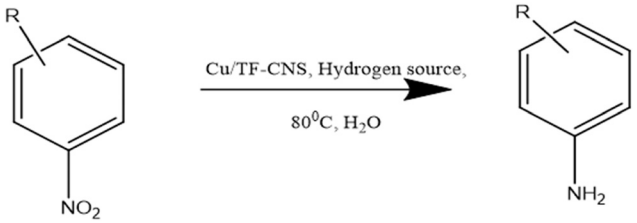

Entry	Substrate	Product (1P to 13P)	Reaction time	Isolated yield
1.	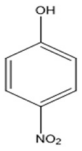	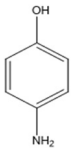	180 min	96%
2.	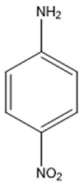	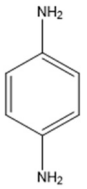	20 min	98%
3.	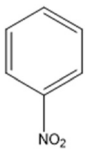	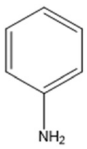	90 min[a]	91%
4.	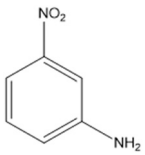	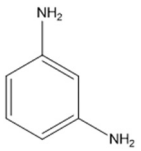	45 min	85%
5.	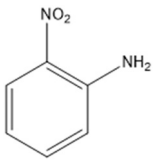	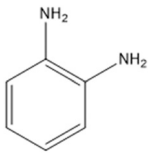	30 min	62%
6.	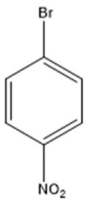	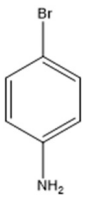	35 min[a]	73%
7.	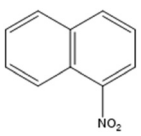	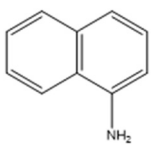	30 min[a]	79%
8.	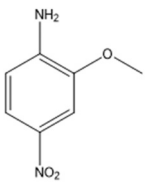	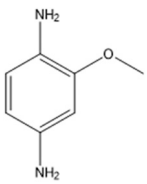	35 min[a]	85%
9.	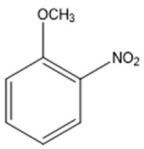	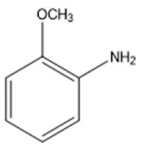	80 min	78%

Table 2 *(continued)*

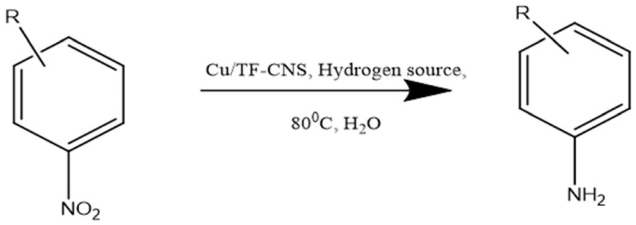

Entry	Substrate	Product (1P to 13P)	Reaction time	Isolated yield
10.	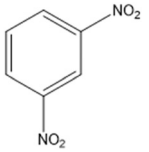	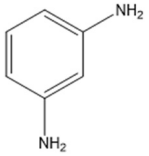	45 min[a]	93%
11.	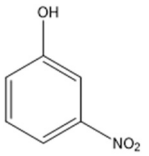	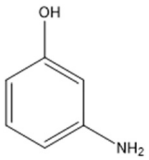	45 min	87%
12.	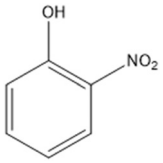	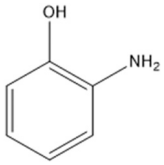	25 min	95%
13.	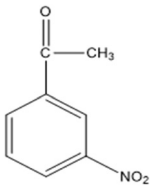	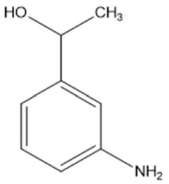	60 min[a]	93%

Reaction conditions: aromatic nitro compound (1.0 mmol), $NaBH_4$ (5 mmol), Cu/TF-CNS (20 wt%) temperature 80 °C, H_2O (3 mL). [a] Solvent: 3 mL, EtOH/H_2O (2 : 1).

onto the catalyst surface.[57] Subsequently, the π-electron cloud of the benzene ring of the nitroarene interacts with the Cu/TF-CNS surface leading to its adsorption.[58] Due to the high electron migration efficiency of Cu^0, it could readily transfer electrons. The released H^+ combines with the oxygens of the nitro group, resulting in the removal of water molecules and the formation of hydroxylamine, which is further dehydrated and ultimately reduced to amino groups.[56,59] Additionally, experimental results indicate that a small amount of Cu_2O/CuO is primarily concentrated on the Cu/TF-CNS surface. The presence of these oxides enhances the reduction reaction by accepting electrons from BH_4^-, reducing Cu(I)/Cu(II) to *in situ* Cu^0.[15] This *in situ* formation of Cu^0 contributes to the acceleration of the catalytic reaction, which may be one of the reasons for the efficiency of the Cu/TF-CNS catalyst.

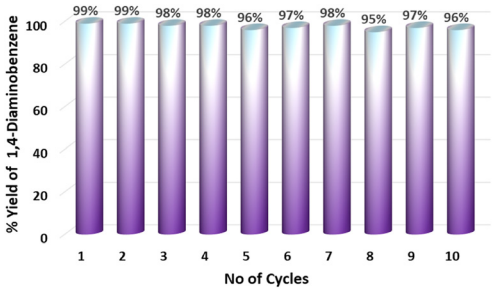

Fig. 4 Recyclability test of Cu/TF-CNS.

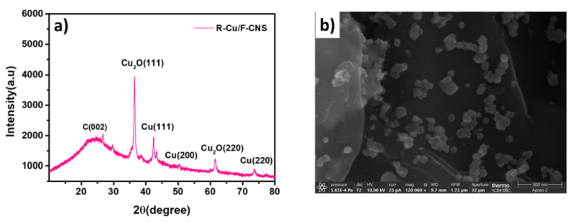

Fig. 5 a) XRD pattern and b) FESEM image of the reused Cu/TF-CNS catalyst (R-Cu/TF-CNS).

Table 3 Comparison of the designed Cu/TF-CNS catalytic system with other reported studies for the hydrogenation of 4-nitroaniline

Entry	Catalyst	Metal loading	Solvent	Hydrogen source	Temp	Time	Yield (%)	Ref.
1.	Pd–gCN	5 mol%	EtOH	$N_2H_4{\cdot}H_2O$	70 °C	4 h	97%	49
2.	Pd@CTF	1 mol%	EtOH/H_2O	NH_4COOH	25 °C	20 min	>99%	50
3.	NiNPs/DNA	2 mol%	H_2O	$NaBH_4$	RT	3 h	>99%	51
4.	Ni@N-CNT	2.4 wt%	MeOH	H_2 (5bar)	80 °C	1.5 h	>99%	52
5.	$CuFe_2O_4$@SiO_2@g-C_3N_4/Cu	35 wt%	H_2O	$NaBH_4$	55 °C	20 min	98%	53
6.	CuO@C	5 mol%	EtOH	$NaBH_4$	RT	2 h	86%%	54
7.	Cu/TF-CNS	4 mol% (20 wt%)	H_2O	$NaBH_4$	80 °C	20 min	98%	Present work

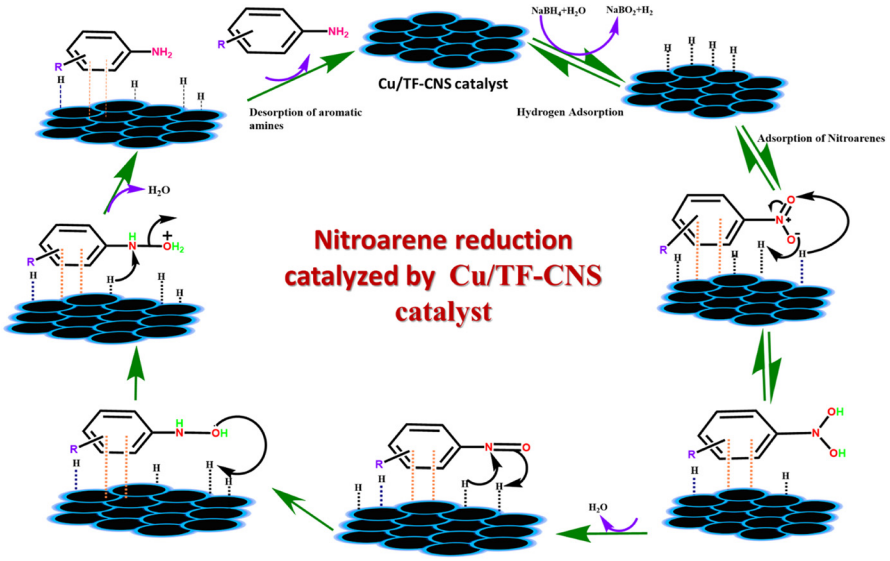

Scheme 2 Plausible mechanism for the Suzuki coupling reaction catalyzed by Cu/TF-CNS

Conclusions

In summary OPL-CNS has been successfully synthesized through a pyrolysis technique utilizing dry palm leaves as a biowaste precursor. Thiol functional groups were introduced into the system *via* a chemical functionalization method to obtain TF-CNS. The incorporation of Cu nanoparticles was achieved through a simple reduction technique to obtain the Cu/TF-CNS catalyst. This synthesized catalyst showed high catalytic activity for a range of nitroarenes producing good yields. The material demonstrated high efficiency and required short reaction times under mild reaction conditions, while utilizing a low loading of non-noble and inexpensive metal like copper (4 mol%) in the catalyst. The presence of thiol functionalities on the porous carbon enhances the stability of the catalyst and also facilitates the uniform dispersion of the metal nanoparticles. As a result, it can be reused for several cycles (up to 10 cycles) without significant loss of its catalytic activity or leaching of the metal into the reaction mixture. Therefore, Cu/TF-CNS presents a promising potential for the reduction of nitro compounds under mild reaction conditions and stands out as an economically viable and environmentally friendly heterogeneous catalyst.

Data availability

The data supporting this article have been included as part of the ESI.†

Author contributions

Apoorva Shetty: conceptualization, methodology, data curation, investigation, validation, writing – original draft, writing – review & editing. Braja Gopal Bag: resources & validation. Uraiwan Sirimahachai: resources & validation. Gurumurthy Hegde: conceptualization, methodology, supervision, validation, funding acquisition, writing – review & editing.

Conflicts of interest

There are no conflicts to declare.

Acknowledgements

One of the authors Apoorva Shetty (IF200410) would like to acknowledge DST-INSPIRE for financial support. The authors would also like to acknowledge SAIF, IIT Bombay and CIL & CIF, CHRIST (Deemed to be University) for instrumental help.

Notes and references

1 M. Gholinejad, Z. Naghshbandi and J. M. Sansano, *Appl. Organomet. Chem.*, 2020, **34**(4), e5522.
2 R. Begum, R. Rehan, Z. H. Farooqi, Z. Butt and S. Ashraf, *J. Nanopart. Res.*, 2016, **18**, 231.
3 H. Göksu, B. Çelik, Y. Yıldız, F. Şen and B. Kılbaş, *ChemistrySelect*, 2016, **1**, 2366–2372.
4 A. H. Romero, *ChemistrySelect*, 2020, **5**, 13054–13075.
5 H. G. Bilgicli, H. Burhan, F. Diler, K. Cellat, E. Kuyuldar, M. Zengin and F. Sen, *Microporous Mesoporous Mater.*, 2020, **296**, 110014.
6 S. Ghosh and B. R. Jagirdar, *Dalton Trans.*, 2018, **47**, 17401–17411.
7 N. Anusuya, C. Pragathiswaran and J. V. Mary, *J. Mol. Struct.*, 2021, **1236**, 130197.
8 P. Prakash, D. De Masi, V. Geertsen, F. Miserque, H. Li, I. N. N. Namboothiri, E. Gravel and E. Doris, *ChemistrySelect*, 2017, **2**, 5891–5894.
9 R. Majumdar, S. Tantayanon and B. G. Bag, *Int. Nano Lett.*, 2017, **7**, 267–274.
10 J. F. de Souza, G. T. da Silva and A. R. Fajardo, *Carbohydr. Polym.*, 2017, **161**, 187–196.
11 K. Zhang, J. M. Suh, J.-W. Choi, H. W. Jang, M. Shokouhimehr and R. S. Varma, *ACS Omega*, 2019, **4**, 483–495.
12 V. S. Sypu, M. Bhaumik, K. Raju and A. Maity, *J. Colloid Interface Sci.*, 2021, **581**, 979–989.
13 M. B. Gawande, A. Goswami, F.-X. Felpin, T. Asefa, X. Huang, R. Silva, X. Zou, R. Zboril and R. S. Varma, *Chem. Rev.*, 2016, **116**, 3722–3811.
14 N. K. Ojha, G. V. Zyryanov, A. Majee, V. N. Charushin, O. N. Chupakhin and S. Santra, *Coord. Chem. Rev.*, 2017, **353**, 1–57.
15 J. Tang, S. Zhang, X. Chen, L. Zhang, L. Du and Q. Zhao, *Catalysts*, 2023, **13**, 956.
16 A. Lazzarini, R. Colaiezzi, F. Gabriele and M. Crucianelli, *Materials*, 2021, **14**, 6796.
17 M. J. Ndolomingo, N. Bingwa and R. Meijboom, *J. Mater. Sci.*, 2020, **55**, 6195–6241.
18 H. N. Hareesh, K. U. Minchitha, K. Venkatesh, N. Nagaraju and N. Kathyayini, *RSC Adv.*, 2016, **6**, 82359–82369.
19 J. H. Bitter, *Catal. Today*, 2023, 114015.
20 A. Bahuguna, A. Kumar and V. Krishnan, *Asian J. Org. Chem.*, 2019, **8**, 1263–1305.
21 E. Lam and J. H. T. Luong, *ACS Catal.*, 2014, **4**, 3393–3410.
22 Z. Liu, B. Zhang, H. Yu, K.-H. Wu and X. Huang, *Front. Chem.*, 2020, **8**, 308.
23 D. T. Bekele, N. T. Shibeshi and A. S. Reshad, *BioEnergy Res.*, 2023, **16**, 1361–1379.
24 B. Basumatary, B. Das, B. Nath and S. Basumatary, *Curr. Res. Green Sustainable Chem.*, 2021, **4**, 100082.
25 F. Kazeminava and Z. Tavakoli, *Mol. Diversity*, 2022, **26**, 1557–1566.
26 Q. Liu, M. Xu, J. Zhao, Z. Yang, C. Qi, M. Zeng, R. Xia, X. Cao and B. Wang, *Int. J. Biol. Macromol.*, 2018, **113**, 1308–1315.
27 M. Lee, B.-Y. Chen and W. Den, *Appl. Sci.*, 2015, **5**, 1272–1283.
28 B. Bowden, M. Davies, P. R. Davies, S. Guan, D. J. Morgan, V. Roberts and D. Wotton, *Faraday Discuss.*, 2018, **208**, 455–470.
29 S. Campisi, C. E. Chan-Thaw and A. Villa, *Appl. Sci.*, 2018, **8**, 1159.
30 Y. Cao, S. Mao, M. Li, Y. Chen and Y. Wang, *ACS Catal.*, 2017, **7**, 8090–8112.
31 D. S. Su, S. Perathoner and G. Centi, *Chem. Rev.*, 2013, **113**, 5782–5816.
32 V. Campisciano, M. Gruttadauria and F. Giacalone, *ChemCatChem*, 2019, **11**, 90–133.
33 R. Zanella, E. V. Basiuk, P. Santiago, V. A. Basiuk, E. Mireles, I. Puente-Lee and J. M. Saniger, *J. Phys. Chem. B*, 2005, **109**, 16290–16295.
34 T. M. Shaffer, S. Harmsen, E. Khwaja, M. F. Kircher, C. M. Drain and J. Grimm, *Nano Lett.*, 2016, **16**, 5601–5604.
35 A. Shetty and G. Hegde, *React. Kinet., Mech. Catal.*, 2024, **137**, 2989–3004.
36 S. Supriya, G. Sriram, Z. Ngaini, C. Kavitha, M. Kurkuri, I. P. De Padova and G. Hegde, *Waste Biomass Valoriz.*, 2020, **11**, 3821–3831.
37 A. Shetty, D. Sunil, T. Rujiralai, S. P. Maradur, A. N. Alodhayb and G. Hegde, *Nanoscale Adv.*, 2024, **6**, 2516–2526.
38 V. S. Bhat, S. G. Krishnan, T. J. Jayeoye, T. Rujiralai, U. Sirimahachai, R. Viswanatha, M. Khalid and G. Hegde, *J. Mater. Sci.*, 2021, **56**, 13271–13290.
39 M. A. Bhosale and B. M. Bhanage, *J. Cluster Sci.*, 2017, **28**, 1215–1224.
40 Z. Li, K. Dai, J. Zhang, C. Liang and G. Zhu, *Mater. Lett.*, 2017, **206**, 48–51.
41 B. Sivaranjini, R. Mangaiyarkarasi, V. Ganesh and S. Umadevi, *Sci. Rep.*, 2018, **8**, 8891.
42 A. Morais, J. P. C. Alves, F. A. S. Lima, M. Lira-Cantu and A. F. Nogueira, *J. Photonics Energy*, 2015, **5**, 057408.
43 G. Qu, J. Zhou, S. Liang, Y. Li, P. Ning, K. Pan, W. Ji and H. Tang, *Mater. Chem. Phys.*, 2022, **278**, 125688.
44 A. Munir, T. ul Haq, A. Qurashi, H. ur Rehman, A. Ul-Hamid and I. Hussain, *ACS Appl. Energy Mater.*, 2019, **2**, 363–371.
45 J. Jiang, X. X. Liu, J. Han, K. Hu and J. S. Chen, *Processes*, 2021, **9**, 680.
46 P. V. F. de Sousa, A. F. de Oliveira, A. A. da Silva and R. P. Lopes, *Environ. Sci. Pollut. Res.*, 2019, **26**, 14883–14903.
47 X. Wang, B. Zhang, W. Zhang, M. Yu, L. Cui, X. Cao and J. Liu, *Sci. Rep.*, 2017, **7**, 1584.
48 V. Fernandez, D. Kiani, N. Fairley, F.-X. Felpin and J. Baltrusaitis, *Appl. Surf. Sci.*, 2020, **505**, 143841.
49 D. Nandi, S. Siwal, M. Choudhary and K. Mallick, *Appl. Catal., A*, 2016, **523**, 31–38.
50 J. Li, L. Zhang, X. Liu, N. Shang, S. Gao, C. Feng, C. Wang and Z. Wang, *New J. Chem.*, 2018, **42**, 9684–9689.
51 M. Niakan and Z. Asadi, *Catal. Lett.*, 2019, **149**, 2234–2246.
52 J. H. Advani, K. Ravi, D. R. Naikwadi, H. C. Bajaj, M. B. Gawande and A. V. Biradar, *Dalton Trans.*, 2020, **49**, 10431–10440.
53 A. Bagherzade, F. Nemati, H. T. Nahzomi and A. Elhampour, *J. Mol. Struct.*, 2019, **1185**, 38–49.

54 V. Vinod Kumar, R. Rajmohan, P. Vairaprakash, M. Mariappan and S. P. Anthony, *Dalton Trans.*, 2017, **46**, 11704–11714.
55 Y. Yan, J. Miao, Z. Yang, F.-X. Xiao, H. B. Yang, B. Liu and Y. Yang, *Chem. Soc. Rev.*, 2015, **44**, 3295–3346.
56 A. A. Kassem, H. N. Abdelhamid, D. M. Fouad and S. A. Ibrahim, *J. Environ. Chem. Eng.*, 2021, **9**, 104401.
57 R. Rai and D. K. Chand, *J. Chem. Sci.*, 2021, **133**, 87.
58 F. Villacañas, M. F. R. Pereira, J. J. M. Orfão and J. L. Figueiredo, *J. Colloid Interface Sci.*, 2006, **293**, 128–136.
59 S. I. El-Hout, S. M. El-Sheikh, H. M. A. Hassan, F. A. Harraz, I. A. Ibrahim and E. A. El-Sharkawy, *Appl. Catal., A*, 2015, **503**, 176–185.